THE JOURNAL OF PHYSICAL CHEMISTRY C

pubs.acs.org/JPCC Article

Ligand Structure Directed Dimensionality Reduction (2D →1D) in Lead Bromide Perovskite

Rangarajan Bakthavatsalam, Muhammed P. U. Haris, Samir R. Shaikh, Amruta Lohar, Ashutosh Mohanty, Dhanashree Moghe, Shivani Sharma, Chinmoy Biswas, Sai Santhosh Kumar Raavi, Rajesh G. Gonnade, and Janardan Kundu*

Cite This: J. Phys. Chem. C 2020, 124, 1888–1897

ABSTRACT: Low dimensional (2D, 1D) lead halide perovskites are currently attracting huge research interest due to their enabling properties. Demonstrating synthetic control on the dimensionality/structure of these perovskites is highly challenging. Dimensionality in these perovskites is largely dictated by the nature/structure and composition of the incorporating ligands and the utilized synthetic conditions. Here, we demonstrate chemical composition based control on reduction of dimensionality (2D → 1D) for lead bromide perovskite utilizing 2-(2-aminoethyl)isothiourea dihydrobromide as a common precursor ligand (Isothio Bromide). Controlling the hydrothermal reaction parameters (temperature, time) at a fixed precursor ratio affords corner-shared, contorted 2D sheet perovskite and corner-shared, contorted, chiral 1D chain perovskite. Such dimensionality reduction leads to contrasting photophysical properties: 1D chain perovskite shows long-lived and self-trapped broad band emission, whereas 2D perovskite shows short-lived, band edge emission with a long tail. Mechanistic studies and single crystal structure analysis reveal the incorporation of the utilized precursor ligand (Isothio Bromide) in 2D perovskite. Surprisingly, the 1D perovskite is found to be chiral ($P2_1$ space group) incorporating 2-(2-aminoethyldisulfanyl)ethanamine and ammonium ions as the achiral ligands generated in situ due to hydrothermal cleavage of the precursor (Isothio Bromide) ligand. Such structural and compositional change of the ligands, which manifests a different hydrogen bonding network in the resultant perovskite structure, plays a decisive role in dictating the final molecular formula and dimensionality/structure of the perovskite which largely controls their photophysical properties.

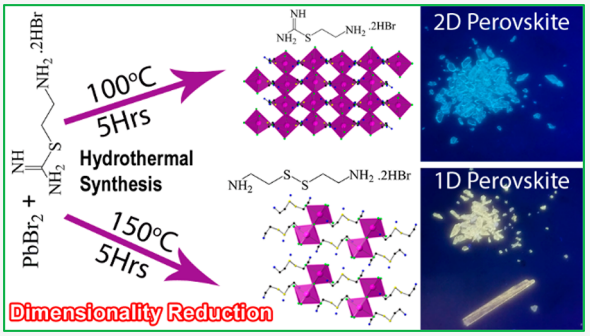

INTRODUCTION

Lead halide perovskite research has seen an exponential growth in the past decade. This paradigm-changing material has received huge attention due to its enabling properties with immense practical applications in solar cells, LEDS, photodetectors, lasers, and X-ray scintillators.[1−4] Three dimensional (3D) lead halide perovskites of the general formula $APbX_3$, consisting of three dimensionally networked metal halide octahedral units, have received extensive research interest due to their defect tolerant nature, ease of synthesis, and unmatched semiconducting and emissive properties.[1] Recently, research efforts have been devoted to lower dimensional perovskites (2D, 1D) wherein the photogenerated excitons are localized in two and one dimension(s) due to the network (structure) of the connectivity of the octahedral unit in two dimension (sheets) and 1 dimension (chains).[5−7] 2D perovskites, with a general formula of L_2PbX_4, has alternating layers of metal halide octahedra forming a sheet and organic ligands (unipositive) with electrostatic and self-assembly forces holding this bulk quantum well structure.[8−10] For the 1D perovskites, generally the metal halide octahedra are connected in a chain structure with organic ligands wrapping around it with electrostatic and self-assembly forces.[7] The reduction of dimensionality in these perovskites (3D → 2D → 1D) largely affects their physical and optoelectronic properties that lead to specific use of low dimensional perovskites for particular applications.[5,6] Unlike 3D perovskites with limited scope of "A" type species (Goldschimdt tolerance factor),[11] lower dimensional perovskites enjoy huge chemical flexibility and diversity owing to their ability to incorporate variety of functional organic molecules as ligands.[8−10] The nature/structure of the ligand has emerged as the key role player in dictating the final dimensionality in these low dimensional lead halide perovskites.[5,6,9,10,12−15] Advancement of synthetic chemistry techniques for lead halide perovskites have now shown that a large library of low dimensional lead halide

Received: November 26, 2019
Revised: December 24, 2019
Published: December 30, 2019

https://dx.doi.org/10.1021/acs.jpcc.9b11033
J. Phys. Chem. C 2020, 124, 1888–1897

Scheme 1. Reaction Scheme Utilized Here for Demonstrating Dimensionality Reduction[a]

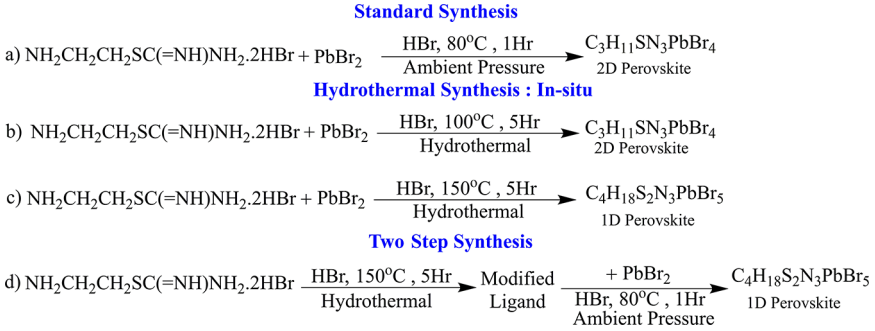

[a]For all of these reactions, the ratio of the ligand to metal halide precursor is kept constant.

perovskites is indeed accessible through rational choice of organic ligands.[10] Karunadasa and co-workers have further shown that 2D perovskites (flat, contorted) with different ligand types show broad band, self-trapped emission (STE) with PL QY ~ 1−10%.[16] Ma and co-workers demonstrated that perovskite dimensionality reduction further augments the PL QY of such broad band, self-trapped emission up to ~25%.[17] Although the fundamental parameter that controls the PL QY of broad-band, self-trapped emission is currently being heavily debated, yet dimensionality reduction plays an observably important role in enhancing the PL QY.[13,18,19] Broad band emission in low dimensional perovskite arises due to transient self-trapping of excitons in the lattice (inorganic, organic) of the semiconductor that relaxes radiatively to the ground state from a broad and structurally distorted excited state of the semiconductor.[16,20,21] The efficiency of this emission is very sensitive to the structure/dimensionality and nature of the ligands/halides.[13,16−19,22] Hence, exploring the relationship of chemical composition to the structure of these low dimensional perovskites holds the key to enhancing the efficiency of the broad-band emission. Synthetic chemistry provides the requisite handle to explore this opportunity to rationally control the chemical composition of the perovskites that ultimately dictates dimensionality reduction. Such a chemical approach would indeed be beneficial in understanding the broad-band emissive properties of these low dimensional perovskite materials.

Many have reported synthetic techniques to achieve dimensionality reduction in metal halide perovskites. Bakr and co-workers utilized water to directly transform films of the three-dimensional (3D) perovskite $CsPbBr_3$ to stable two-dimensional (2D) perovskite-related $CsPb_2Br_5$. It has been reported that the nanocrystals of Cs_4PbBr_6 can be converted to $CsPbBr_3$ by the extraction of CsBr with water.[23−27] Yella and co-workers demonstrated water vapor induced reversible transformation of 0D $MA_4PbX_6{\cdot}2H_2O$ (X = Br, I) to 3D $MAPbX_3$ perovskite.[28] Mohammed and co-workers have demonstrated that the introduction of pyridine during the synthesis of methylammonium lead bromide ($MAPbBr_3$) perovskite nanocrystals can transform three-dimensional (3D) cubes into two-dimensional (2D) nanostructures.[29] Ma and co-workers have demonstrated photoinduced dimensionality reduction (1D → 0D) for tin bromide perovskites.[30] Billing and co-workers have demonstrated changes in dimensionality (2D, 1D) when utilizing different diamine ligands.[12] Jin and co-workers demonstrated the reduction of dimensionality (2D, 1D) utilizing symmetric and asymmetric diamines.[31] Recently, Kundu and co-workers demonstrated change in dimensionality (2D, 1D) when different reaction conditions were utilized for the synthesis of the perovskites.[32] These observations of change in structure/dimensionality of perovskites brought about by utilizing ligands with different structures and different chemical synthetic routes provide huge opportunity for scientific research on material design and tailoring their optoelectronic properties.

Here, we demonstrate dimensionality reduction and associated changes in optical properties of lead bromide perovskite from contorted 2D sheet to contorted, chiral 1D chain structure through controlled hydrothermal synthesis using 2-(2-Aminoethyl)isothiourea dihydrobromide (hereafter termed as Isothio Bromide) as the precursor organic ligand. Controlling the hydrothermal reaction parameters (temperature, time) using the Isothio Bromide ligand and $PbBr_2$ salt (at a fixed ratio) affords corner-shared, contorted 2D sheet perovskite of $NH_3CH_2CH_2SC(=NH_2)NH_2$ $PbBr_4$ at (100 °C, 5 h) and corner-shared contorted chiral 1D chain perovskite of $(NH_3CH_2CH_2SSCH_2CH_2NH_3)$ $PbBr_5.NH_4$ at (150 °C, 5 h). Such a change in dimensionality/structure largely affects the optical properties: 2D perovskite shows long-tailed band edge emission while the 1D perovskite shows self-trapped broad band emission. Single crystal structure analysis clearly shows that for the 2D perovskite the incorporated ligand is 2-(2-aminoethyl)isothiourea dihydrobromide, whereas for the 1D chain perovskite the incorporated ligand is ammonium ion and 2-(2-aminoethyldisulfanyl)ethanamine (reaction Scheme 1) generated in situ hydrothermally from Isothio Bromide precursor ligand. This in situ conversion of the Isothio Bromide ligand to modified ligand, as probed further using a two-step hydrothermal synthesis method (reaction Scheme 1d), was found to be driven by the chosen temperature and reaction time. Such structural change of the ligand, which manifests a different hydrogen bonding network in the resultant 1D perovskite structure, plays a decisive role in dictating the final dimensionality/structure of the perovskite which largely controls their contrasting photophysical properties.

EXPERIMENTAL SECTION

Materials and Methods. Lead (II) bromide (99%) and acetone were purchased from Sigma-Aldrich. 2-(2-Aminoethyl) isothiourea hydrobromide and HBr (47%) were purchased from TCI Chemicals. All chemicals were utilized without further purification.

Standard Synthesis of 2D $IsoPbBr_4$ Perovskite. Three mmol of 2-(2-aminoethyl)isothiourea dihydrobromide, and

https://dx.doi.org/10.1021/acs.jpcc.9b11033
J. Phys. Chem. C 2020, 124, 1888−1897

lead bromide ($PbBr_2$) (1:1) were dissolved in 20 mL HBr by heating at 80 °C for 1 h and was allowed to cool slowly to obtain colorless crystals. They were filtered and washed thoroughly with acetone and dried under vacuum overnight. This synthesis protocol is adapted from the report by Lin et al.[33]

Hydrothermal in Situ Synthesis of 2D and 1D Perovskite. Three mmol of 2-(2-aminoethyl)isothiourea dihydrobromide and lead bromide ($PbBr_2$) (1:1) were mixed with 20−25 mL HBr stirred for 5 h. The resulting mixture was transferred to a Teflon lined stainless steel hydrothermal vessel. The vessel was then sealed and heated in an oven. The temperature and reaction time were varied to obtain different products (see Scheme 1).

Two Step Synthesis of 1D Perovskite. Three mmol of 2-(2-aminoethyl)isothiourea dihydrobromide was dissolved in 15 mL HBr and transferred to a Teflon lined stainless steel hydrothermal vessel. It was then heated at 150 °C for 5 h to obtain a pale brown solution. The solution was then transferred to a 50 mL round-bottom flask containing 3 mmol $PbBr_2$ in 10 mL of HBr. The resultant mixture was heated at 80 °C until dissolution and then cooled to obtain colorless crystals. The crystals were filtered and washed thoroughly with acetone and dried under vacuum overnight.

Characterization. UV−vis absorbance was performed in a Shimadzu UV−vis−NIR 3600Plus spectrometer. Steady State PL and lifetime was measured using an Edinburgh FS5 spectrophotometer. PXRD patterns were recorded using a PANalytic X'Pert Pro using Copper Kα radiation (λ = 1.5406 Å). TGA measurements were performed using a TAG system (Mettler-Toledo, Model TGA/SDTA851e) and samples were heated in the range of 25−800 °C at a heating rate of 10 °C/min under nitrogen atmosphere. For steady-state power dependent measurement, the sample was excited with the 355 nm line of an Innolas Picolo AOT Nd:YAG laser using a variable neutral optical density filter, where the power was varied. The emission was collected in the reflection mode using an Andor-iCCD spectrometer. Absolute quantum yield measurement was carried out in a Horiba JOBIN YVON Fluoromax-4 spectrometer with a calibrated integrating sphere attachment. Low-temperature PL measurements were performed on a home-built PL set-up consisting of an excitation monochromator (Jobin Yvon Triax 180), an emission monochromator (Jobin Yvon iHR 320) and photomultiplier tube (PMT) as the detector with xenon lamp (450 W). ^{1}H NMR was recorded in DMSO-d6 as solvent using a Bruker Avance DPX 200 MHz spectrometer referenced to external $SiMe_4$ standard. Single crystal X-ray intensity data measurements were carried out on a Bruker D8 VENTURE Kappa Duo PHOTON II CPAD diffractometer equipped with Incoatech multilayer mirrors optics. More details about data collection and analysis of single crystal structure elucidation experiments is provided in the Supporting Information, SI.

RESULTS AND DISCUSSION

Standard synthesis (reaction Scheme 1a) using Isothio Bromide ligand and $PbBr_2$ salt in HBr solvent, upon crystallization, leads to the formation of contorted ⟨110⟩ oriented layered $C_3H_{11}SN_3PbBr_4$ perovskites in agreement with an earlier report.[33] This synthesis when performed hydrothermally at 100 °C, 5 h (reaction Scheme 1b) leads to the formation of the same contorted ⟨110⟩ oriented 2D sheet perovskite ($C_3H_{11}SN_3PbBr_4$) single crystals. High quality single crystals can be easily obtained utilizing this hydrothermal approach. Single crystal structure analysis of the product (CCDC1942429), shown in Figure 1a,b below,

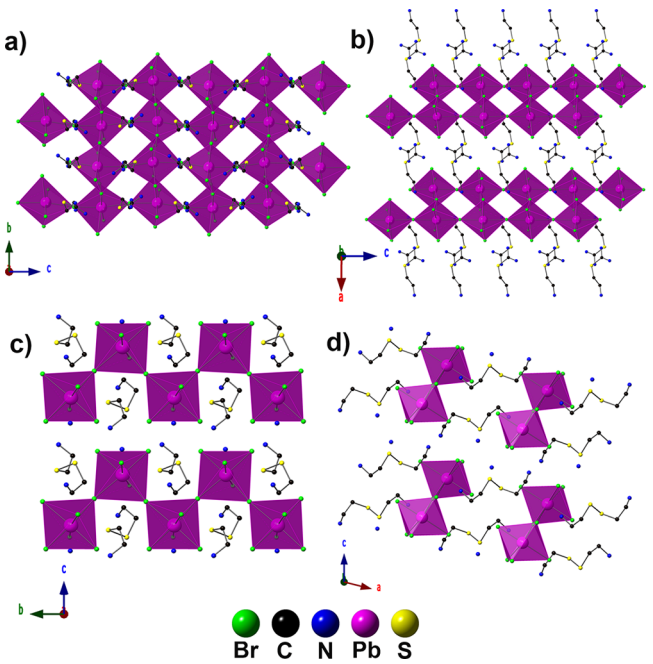

Figure 1. Single crystal structure of contorted 2D perovskite (a,b), and corner shared, chiral 1D chain perovskites (c,d). H atoms have been omitted for clarity.

obtained using reaction Scheme 1b, shows that the resultant perovskite is indeed a ⟨110⟩ oriented 2D layered structure in close agreement with the results of Lin[33] et al. The asymmetric unit, as shown in SI Figure S1, clearly shows the presence of Isothio Bromide as the incorporated ligand in this 2D perovskite structure. The presence of the primary amine and the formamidinium moiety along with Pb−Br−Pb bridging angles deviating from linearity largely dictate the contorted 2D sheet structure. This structure is also characterized by large distortions in the Pb−Br bond lengths and octahedral tilts that affect its optical properties (discussed later). The crystal structure shows a network of hydrogen bonding involving the primary amine and the formamidinium group that leads to the alternating layers of ligands in between the metal halide octahedral sheets. The successful hydrothermal synthesis of 2D peorvskite shows that although the thermodynamics and kinetics of synthesis under hydrothermal conditions are very different from the standard synthesis process, yet the hydrothermal synthesis of 2D perovskites is indeed a viable route.

Interestingly, the hydrothermal reaction conditions when set to 150 °C, 5 h as depicted in reaction Scheme 1c, affords a new product that has strikingly different optical properties (discussed later) than the contorted ⟨110⟩ oriented 2D perovskites obtainable through reaction Scheme 1b. The single crystal structure analysis of the product, as shown in Figure 1c,d, clearly shows the corner shared, contorted, 1D chain like perovskite structure that extends along the *b* axis surrounded by the ligand. The 1D perovskite crystallizes in a monoclinic crystal system with $P2_1$ space group (CCDC1942428). These contorted 1D chains have the bridging angle (Pb1−Br5−Pb1) of 169.8(1) largely deviating from linearity. This changeover in

https://dx.doi.org/10.1021/acs.jpcc.9b11033
J. Phys. Chem. C 2020, 124, 1888−1897

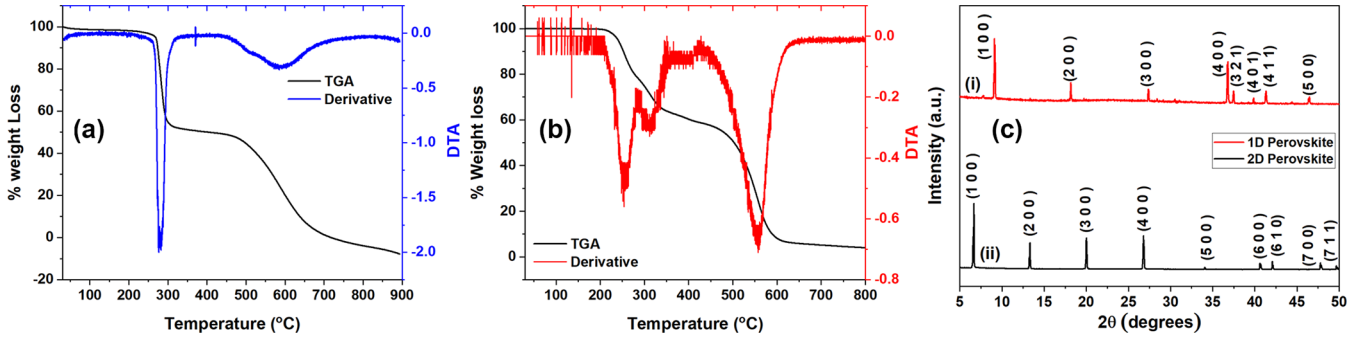

Figure 2. Thermogravimetric analysis (TGA) of hydrothermally synthesized (a) 1D perovskite, (b) 2D perovskite, (c) PXRD pattern of crystals of hydrothermally synthesized (i) 1D perovskite and (ii) 2D perovskite (patterns offset for clarity).

dimensionality/structure from 2D/sheets →1D/chain is achieved through changes in the hydrothermal reaction temperature without any modification of the reactant ratio. Excitingly, the nature of the incorporated ligand in this 1D perovskite is strikingly different from Isothio Bromide ligand used as the precursor. The modified ligand that is incorporated in this 1D perovskite is 2-(2-aminoethyldisulfanyl)ethanamine, as depicted in the asymmetric unit (SI Figure S1). Additionally, ammonium ions are identified in the crystal structure that work as charge balancing counterions. Intuitively, this modified ligand can be thought of as being generated in situ due to hydrothermal cleavage of the Isothio Bromide ligand and dimerization due to S−S bond formation (reaction Scheme 1). Further mechanistic understanding supporting the above in situ generation of the modified ligand and identification of the charge balancing ammonium ion is discussed in detail later in this report.

The change in dimensionality/arrangement of inorganic moiety is greatly affected by the composition and structure of the ligand through hydrogen bonding and steric hindrance. The distance between sulfur to bromine atom is 4.107 Å for the 1D perovskite, larger than that in the 2D perovskite (3.510 Å). This suggests that the sulfur might not have a direct role in the arrangement of the 1D structure as it does in the case of contorted ⟨110⟩ oriented 2D perovskite.[33] Utilizing the 1D ligand directly in the standard synthesis reaction yields a 2D ribbon[34,35] like perovskite rather than a 1D structure. This indicates that the additional ammonium ions generated from the breakdown of isothio urea ligand is crucial in directing a purely 1D perovskite structure: small unipositive ammonium ions charge balance by inserting along the inorganic chain framework. The 1D ligand, 2-(2-aminoethyldisulfanyl)-ethanamine, is oriented along *a* axis. Both the terminal amines of the 1D ligand form hydrogen bonds with different Br atoms. One of the terminal ammonium group (N1) forms hydrogen bonding with two Br5 atoms of the same chain. The other terminal ammonium (N2) forms hydrogen bonding with two different bromine atoms (Br2 and Br4) across two different but adjacent chains of $PbBr_6$ octahedra. The hydrogen to Br distances are from 2.454 to 2.748 Å indicating stronger hydrogen bonding interactions. In the 1D perovskite, the distance between the Br (1), Br (4), and N (3) is 3.34 Å and 3.36 Å, respectively, which is similar to the N to Br distances of 2D ligand as well as 1D ligand nitrogens to the respective bromines. This arrangement of ligand and the presence of a smaller ammonium ion effectively isolate the PbBr octahedra into forming a pure 1D chain rather than a 2D sheet like structure.

Additionally, the 1D perovskite is determined to crystallize in a chiral space group $P2_1$ with a 2_1 screw axis of symmetry that gives rise to the helical arrangement of the ligand and metal halide octahedral unit. While none of the starting materials or the 1D ligand are chiral, the observed chirality in the single crystals arises mainly due to the conformational helical chirality of the disulfide ligand. The incorporated modified ligand in the solid state is known to exhibit skewed enantiomeric conformations due to low rotational barrier around the C−S−S−C dihedral angle.[36,37] In the literature, there are many reports of 2D and lower dimensional perovskites that utilize a particular chiral isomer of the ligand to impart chirality in perovskites,[38−41] there are very few reports of perovskites that are chiral by the arrangement of its structure alone[36,37,42] as observed in our 1D perovskite structure here. Temperature dependent optical and single crystal structure characterizations, probing the chirality of the 1D perovskites, are being pursued and are beyond the scope of the present work.

The observed reduction of the dimensionality (2D → 1D), guided by the in situ change of ligand structure, shows dramatic differences in their structures as discussed above. Thermogravimetric analysis (TGA) of the 2D and 1D perovskites fabricated as per reaction Scheme 1b,c, respectively, as shown in Figure 2a,b, highlights interesting differences. For the 1D perovskite, the ligand loss feature is sharp and centered at ∼280 °C while for the 2D perovskite, the ligand loss feature is broad spanning 250−310 °C. Such broad weight loss peak for the Isothio Bromide ligand might suggest changes in the ligand structure over the 250−310 °C temperature range. This broad weight loss peak of the Isothio Bromide ligand in 2D perovskite is very similar to the TGA spectra for Isothio Bromide ligand alone as shown in SI Figure S2. These observations indicate that indeed the Isothio Bromide ligand, upon thermal treatment, can lead to decomposition and structure modification. The PXRD for the crystals of 2D perovskites synthesized according to reaction Scheme 1b, as presented in Figure 2c (ii), shows a characteristic pattern of equally spaced lines in consonance to the layered 2D structure. The calculated interplanar *d*-spacing value (1.32 nm; 2θ periodicity = 6.7°) is in consonance to the prior report.[33] However, for the 1D perovskite synthesized as per reaction Scheme 1c, shows XRD pattern (Figure 2c (i)) that is different than 2D perovskites. The PXRD pattern of 1D perovskite sample (ground powder) match well with the XRD pattern simulated from its single crystal data (SI Figure S3) demonstrating phase purity.

https://dx.doi.org/10.1021/acs.jpcc.9b11033
J. Phys. Chem. C 2020, 124, 1888−1897

Dimensionality reduction remarkably affects the photophysical properties of these low dimensional perovskites. Steady state optical properties (absorbance, PL, PLE) of the 2D perovskite synthesized through reaction Scheme 1b, presented in Figure 3a, match closely to the ones reported

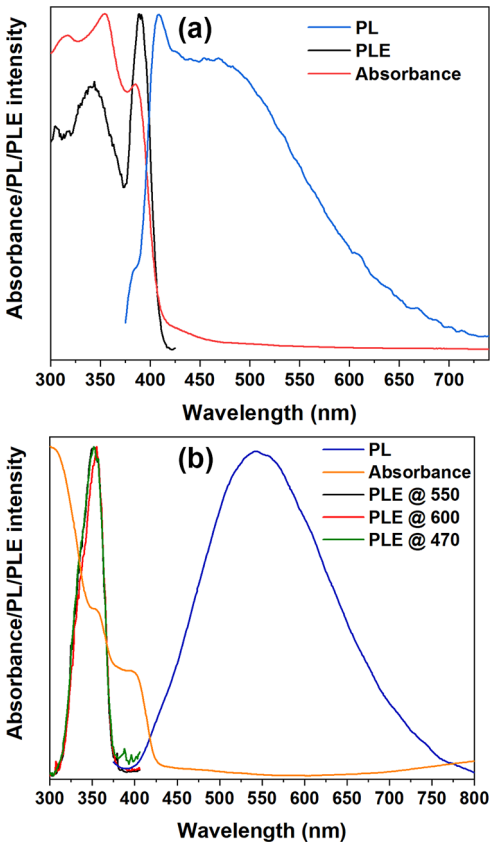

Figure 3. Optical properties of hydrothermally synthesized (a) 2D perovskite and (b) 1D perovskite showing broad band emission. For the utilized polycrystalline samples, the PL excitation wavelength is set at 360 nm and PLE for (a) is collected at 435 nm and for (b) is collected at 470 nm, 550 nm, and 600 nm. For comparison, intensity maximum of each curve is normalized to unity.

by Lin[33] et al. The photoluminescence (PL) spectra show a sharp band edge emission (~415 nm) along with a long tail that extends over the visible range. This sharp PL band, closely overlapping with the absorption profile, arises due to band edge recombination process wherein the photogenerated free excitons (FE) relax back to the valence band. The PL band peak position is in general agreement with the reported band edge emission of many 2D lead bromide perovskites.[43] The contorted nature of the 2D perovskite supports distortions (in plane, out of plane, within an octahedron). Such distortions in contorted 2D perovskites are well-known to support transient excited state defects that are generated upon band edge photoexcitation (generation of self-trapped excitons or STEs).[43] Given the contorted nature of the 2D perovskite with appreciable distortions in the crystal structure (see SI Table S1), it is very likely that the broad emission here arises due to STEs. This is in agreement with the same assessment by Karunadasa and co-workers.[16] Moreover, photoluminescence excitation (PLE) spectra (collected at 435 nm) match closely with the absorption profile as shown in Figure 3a indicating that the tailed emission arises due to band edge excitation and no other emitting species (permanent defects) are involved. It is likely that the there exists a thermal equilibrium between the FE and STEs that interconvert rapidly (at room temperature) and hence shows both sharp band edge emission and a shoulder broad tailed emission in the contorted 2D perovskite.

The optical properties of the 1D perovskites are presented in Figure 3b. The emission profile is very broad extending over the entire visible range with no observable sharp band edge peak. This broad emission shows appreciable Stokes shift. The PLE profile collected across the broad emission band remains unchanged indicating only one kind of emissive species result in the broad emission. Further, steady state and time-resolved photoluminescence measurements were carried out to gain insight into the nature of this broad emissive band for the 1D perovskite.

The lifetime measurements of the 2D perovskite as synthesized through the standard process (reaction Scheme 1a) reveal biexponential decay curves with 5 ns (weightage: 74%) and 14 ns (weightage: 26%) time constants. Very similar decay curves are obtained for the 2D perovskite synthesized hydrothermally through reaction Scheme 1b with time constants of 4.5 ns (weightage: 54%) and 12 ns (weightage: 46%) as shown in Figure 4 a. Moreover, the lifetimes do not change across the long tailed emission band (see SI Table S2). Interestingly, for the 1D perovskite synthesized through reaction Scheme 1c, the observed lifetimes are lengthened with a major lifetime component of ~30 ns. This lengthened time constant in the 1D system is reflective of the changes in the electronic confinement/dimensionality. The time constants

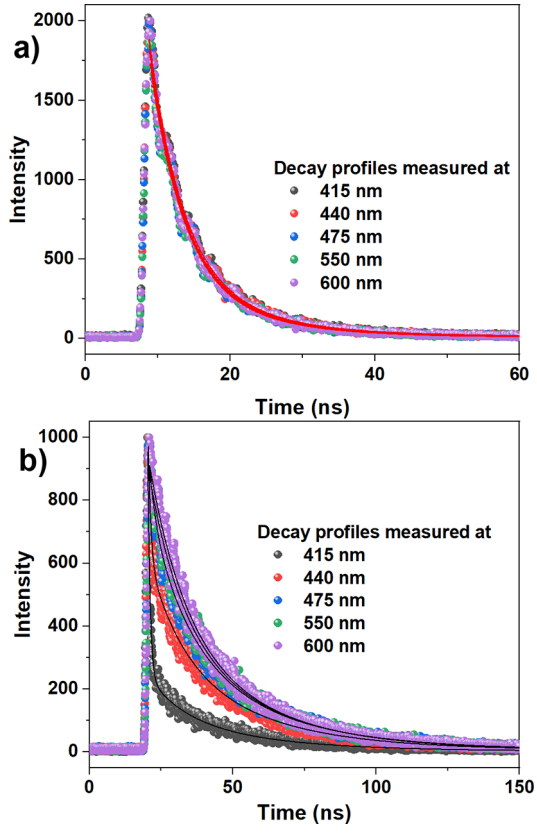

Figure 4. Photoluminescence lifetime decay profile of polycrystalline samples of hydrothermally synthesized (a) 2D perovskite and (b) 1D perovskite. (Excitation wavelength is 330 nm for all samples, while collection wavelengths are as indicated in the respective panels).

https://dx.doi.org/10.1021/acs.jpcc.9b11033
J. Phys. Chem. C 2020, 124, 1888−1897

remain unaltered across the broad emission profile of the 1D system (see SI Table S2 and Figure S4) indicating the unique origin of the broad emission.

Low dimensional perovskites (2D, 1D) have been known to manifest broad band emission across the visible range. Such broad band emission in low D perovskites have been attributed to the transient generation of self-trapped excitons that emit from an excited distorted electronic state of the semiconductor.[16] Here, the reported 1D perovskite shows intrinsic broad-band emission with low PL QY of ~5%. This broad band emission could arise due to defects in the system.[16,44,45] However, the following observations suggest that the emission is intrinsic in nature with one type of emitting species. PLE curves collected at various emission wavelengths across the broad band emission in 1D perovskites are all identical (Figure 3b). Time resolved PL measurements of 1D perovskites, as discussed above, reveal that the major lifetime component is long-lived (~30 ns) and almost remains unchanged across the 440−600 nm broad emission band (see SI Table S2 and Figure S4). To eliminate the hypothesis that surface defects are contributing to the observed broadband emission, grinding and annealing experiments were performed where the crystals were ground for 15−30 min, and annealed for 30−60 min at 100 °C. For the samples that underwent 30 min of grinding and 60 min of annealing, the PL profile of the broad emission remained unchanged. Such grinding and thermal annealing experiments (SI Figure S5) showing no change in the PL band profile indicates that the broad emission is not due to trap states arising from surface defects. Further, we studied the dependence of intensity of the broad band emission on excitation intensity. If the emission arises from permanent defects, then PL saturation is expected as the defect/traps are filled at higher pump fluences.[46,47] SI Figure S6 shows that the PL intensity increases linearly with an excitation power density from 0.3 to 1000 mW/cm^2 at room temperature with no signs of PL saturation. This linear behavior with no observable saturation suggests that emission does not arise from permanent defects. All of these results indicate that defects are not responsible for the broad band emission. In order to gain further insight into the mechanism of this broad band emission in 1D perovskite, low temperature PL measurements were carried out (SI Figure S7). Figure 5a shows the change in integrated PL intensity and bandwidth (fwhm) at different temperatures for the polycrystalline powder of 1D perovskite. The broad band PL intensity increases with the lowering of the temperature from 298 to 180 K. With further temperature lowering the PL intensity starts to decrease. However, across the temperature range investigated, the narrow band edge emission is not observable, and the PL profile is dominated by broad band emission. Such nonemergence of the narrow band edge emission has been documented for variety of lower dimensional perovskites (2D, 1D, 0D).[48−50] A clear understanding of this observation is, however, currently unavailable. Also, the bandwidth (fwhm) of the broad emission increases monotonically as the temperature is raised. Such dependence of PL intensity has been observed in other materials and is due to the thermal equilibrium between excitons in the conduction band state of the band edge excitonic emission (free exciton FE) and the self-trapped emission (STE) states.[16] The observed increase in the intensity of the broad STE emission as the temperatures are lowered can be understood as arising from a thermally driven back transfer from the STE to the FE state, which becomes more difficult at lower temperatures.[16]

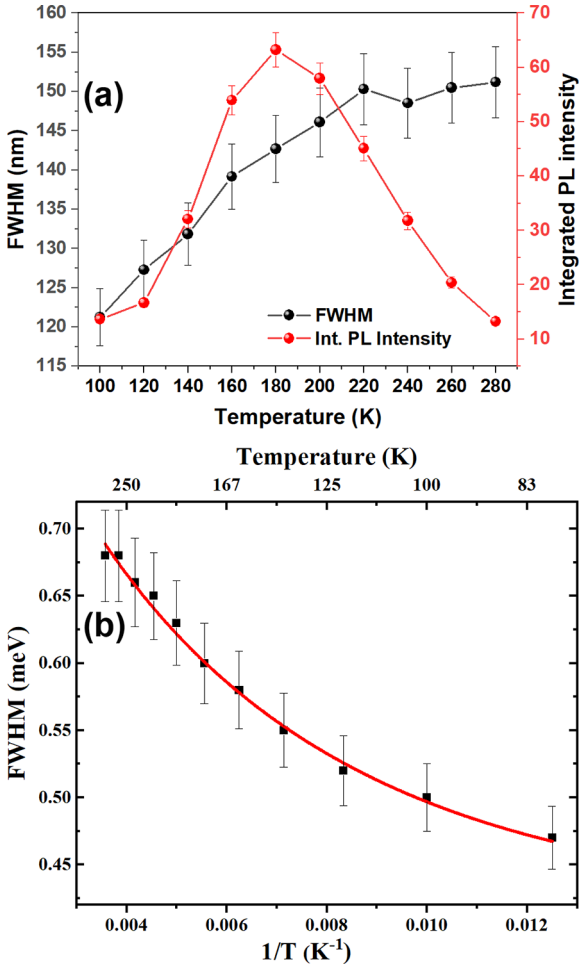

Figure 5. (a) Temperature dependence of integrated PL intensity and bandwidth of the broad band emission of 1D perovskite; and (b) fitting of fwhm as a function of inverse temperature for the 1D perovskite.

Then, at low temperatures, the carriers are less able to surmount the activation barrier from the FE to the STE states leading to a decrease in broad STE emission PL.[16] Moreover, the phonon modes (inorganic and/or organic), which couple with electronic excitation to generate STE, have their own temperature dependence.[51] Bandwidth (fwhm) of the broad emission increases monotonically as the temperature is raised. The dependence of fwhm (Γ) on inverse temperature, as shown in Figure 5b, can be fitted to an equation[52] relating coupling of electronic excitations with the longitudinal optical lattice phonons as follows:

$$\Gamma(T) = \Gamma_0 + \Gamma_{\text{Phonon}}(e^{(E_{\text{LO}}/k_{\text{B}}T)} - 1)^{-1} + \Gamma_{\text{inhomo}}e^{-E_{\text{b}}/k_{\text{B}}T} \quad (1)$$

Here, Γ_0 represents fwhm at 0 K, Γ_{phonon} represents electron−phonon coupling, E_{LO} represents energy of longitudinal optical phonon mode, Γ_{inhomo} represents inhomogeneous broadening, and E_{b} is binding energy of trapped states. The fitting and its associated parameters (SI Figure S8) reflects strong electron−phonon coupling with E_{LO} = 175 cm^{-1} in close agreement to low frequency Raman stretching mode of Pb−Br bonds[18,48] of inorganic metal halide framework suggesting STE localization on metal halide octahedral framework. Strong vibronic coupling between excitons and the lattice phonon can cause

https://dx.doi.org/10.1021/acs.jpcc.9b11033
J. Phys. Chem. C 2020, 124, 1888−1897

broadband emission due to the formation of transient excited state that is highly distorted with respect to the ground state. Such self-trapped excitons are reported to be present in 2D and 1D perovskites.[8,13,16−18,32] The observed linear power dependence, results of the grinding and annealing experiments, time-resolved PL experiments, low temperature PL studies, and the observed similarity to reported cases of self-trapping in 2D and 1D perovskites are consistent with emission from such photogenerated transient self-trapped excited states[53] in our 1D perovskite.

As presented in Figure 3a, the optical properties of the ⟨110⟩ oriented contorted 2D perovskite matches well with the optical properties reported by Lin et al.[33] However, the nature of the long tailed emission band in the contorted 2D perovskite has not been scrutinized. As mentioned earlier in this work, we believe that the long tailed emission can arise from thermal equilibrium between the FE and the STE states in this highly distorted layered perovskite. In order to gain further understanding, steady state low temperature photoluminescence measurements were carried out utilizing polycrystals of 2D perovskites synthesized through Scheme 1b. The PL profiles at different temperatures are shown in SI Figure S9a,b. With the decrease in temperature (room temperature to 80 K), the free exciton high energy emission peak blue shifts while the low energy broad tailed emission red-shifts. Significantly, the broad tailed emission red-shifts by ∼60 nm upon decrease of temperature from room temperature to 80 K. The broad emission gains intensity as the temperature is decreased. The observed relative increase of the broad emission with respect to the narrow emission as temperature is decreased is understandable in terms of thermal equilibrium and interconversion of excitons between the FE state and the broad emitting STE state. The broad peak undergoes peak narrowing as the temperature is lowered as shown in Figure S9c. The fwhm can be fitted to eq 1 highlighting the significant role of the electron−phonon coupling in shaping the broad band PL profile. The fitted parameter of E_{LO} is in general agreement with the reported values for other lead bromide based perovskites showing broad STE based emission. However, it is important to note that the observed red-shift of the broad emission band is huge (∼60 nm) and needs further investigation.

With the understanding of STE based broad band emission in 1D perovskites, a comparative analysis of the lifetime decay data of the 2D and 1D perovskites can provide some insight. Similar lifetimes across the entire emission band for 2D perovskite is observed (SI Table S2). Such similarity of lifetimes in 2D perovskite could arise due to the possible existence of thermal equilibrium between the free exciton (FE) states and the self-trapped exciton states (STEs) at room temperature with rapid interconversion between the FE and STE states. Such similarity of lifetime across the PL emission profile is in line with previous report on contorted 2D perovskites that show STE based broad emission.[54] The different time components (listed in SI Table S2) are tentatively rationalized in terms of FE (τ_1) and STE (τ_2) emissive excitons for the 2D perovskite. The weightage of the operative emission channel, as obtained through fitting parameters A_1 and A_2, suggests that for the 2D perovskite the band edge recombination is dominant and the self-trapping at room temperature is weak. However, for 1D perovskite, with lower dimensionality supporting strong/modest self-trapping, contrasting lifetimes of the band edge FE states (τ_1) and STE states (τ_2) are observed. For lifetimes collected close to the band edge range (410−440 nm emission), the observed FE lifetimes are in the range of ∼10 ns with equally dominant STE based ∼30 ns emission channel. When the lifetimes are collected in the 480−600 nm emission range, an increased weightage of the self-trapped channel is observed suggesting that the dominant relaxation occurs through STE emission pathway even at room temperature. The dominant STE based emission channel is likely to tip the thermal interconversion equilibrium between the FE and STE states toward STE emission albeit with observable increase of band edge FE lifetime. The band edge FE lifetime for 1D and 2D perovskite is largely dictated by the dimensionality/structure and octahedral connectivity in the corresponding perovskites. Noteworthy here, the exciton dynamics in 2D and the 1D system, as inferred from lifetime data above, are more complicated, and further work is needed to investigate the nature and mechanism of the STEs (extrinsic, intrinsic) that causes broad band emission in these perovskites.

Synthetically, tuning the hydrothermal reaction conditions affords the change in dimensionality/structure of the perovskite. In order to gain further mechanistic understanding into this, various hydrothermal syntheses were attempted with different reaction conditions (albeit with the same fixed ratio of ligand to metal halide precursor). Essentially, the temperature and time for the hydrothermal reactions were varied (temperature from 100 to 150 °C; time from 2 to 5 h). In all of these cases, perovskitic products could be isolated, and their optical properties are presented in Figure 6a. It is clear that contorted 2D perovskite results when the hydrothermal

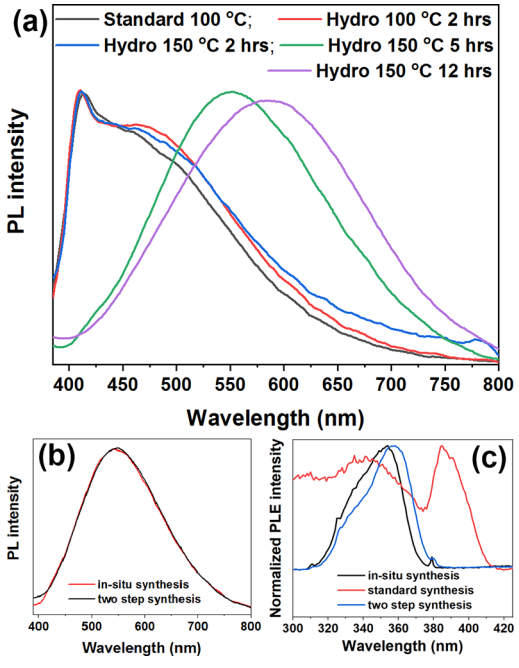

Figure 6. (a) PL profile of perovskites synthesized at different hydrothermal conditions showing dimensionality reduction (2D → 1D); (b) comparison of PL and (c) PLE profile of perovskites synthesized using in situ and two step synthesis. For the utilized polycrystalline samples, PL excitation wavelength is set at 360 nm and PLE for (c) is collected at 435 nm for 2D perovskite (standard synthesis) and 550 nm, for 1D perovskite (in situ, two step synthesis). For comparison, the intensity maximum of each curve is normalized to unity.

https://dx.doi.org/10.1021/acs.jpcc.9b11033
J. Phys. Chem. C 2020, 124, 1888−1897

reaction conditions are set for 2 h at 100 and 150 °C. The recorded PL spectra from these samples are very similar to PL of 2D perovskite synthesized through standard method (reaction Scheme 1a). Interestingly, when the hydrothermal reaction time is lengthened to 5 or 12 h at 150 °C, the PL emission profile becomes broad covering the visible region. This clearly suggests that both hydrothermal reaction temperature and reaction time are relevant factors that govern the final dimensionality of the crystallized perovskite. In order to scan the synthetic parameter phase space relevant for the dimensionality reduction, several one-step hydrothermal reactions were carried out by varying the temperature and time of the reaction. Perovskitic products obtained through such efforts are optically characterized, and the results are presented in SI Figure S10. This suggests that the reduction of the dimensionality occurs when hydrothermal reaction conditions are set to the following: temperature >150 °C, and time >4 h (SI Table S3).

Since such a change in the dimensionality is observed to be associated with a remarkable change in the incorporated ligand structure and composition (Isothio Bromide → modified ligands), a two-step synthesis method (reaction Scheme 1d) was utilized for rationalizing the formation of the 1D perovskite. Initially Isothio Bromide ligand was treated hydrothermally in HBr at 150 °C, 5 h in the absence of any metal salt. This solution was then utilized for dissolving the metal halide salt, heated to 80 °C in open ambient pressure (nonhydrothermal), and allowed to cool naturally for crystallization. This process afforded a perovskite product whose optical properties are presented in Figure 6b,c. The PL profile of this two-step synthesized perovskite matches very well with the emission of perovskite synthesized using the in situ reaction Scheme1c. Further, PLE spectra of the two-step synthesized perovskite compare well with the PLE spectra of in situ synthesized perovskite. These two PLE spectra having a spectral feature centered at ∼350 nm are blue-shifted from the PLE spectral feature (at ∼390 nm) for the 2D standard perovskite indicating dimensionality reduction. The results from the two-step synthesis process suggest that indeed there is in situ hydrothermal generation of the modified ligand which then further reacts to form the 1D perovskite. This is in agreement to the qualitative similarity of the TGA data of the Isothio Bromide ligand and the TGA data of 2D perovskite, where the decomposition of the ligand occurs in a two step manner rather than a single step indicative of a chemical transformation/cleavage. Important to note here is that the complete sequence of reaction events that lead to the generation of modified ligand, free ammonium ions, and other moieties from hydrothermal cleavage of Isotho Bromide ligand is not addressed in this work. However, the presence of the small ammonium ions as the charge balancing counterion in 1D perovskite is confirmed through single crystal structure and ^{1}H NMR analysis. NMR of standard ammonium chloride salt presents triplet peaks in 7.2−7.8 ppm region. This triplet is indicative of J (^{14}N, ^{1}H) coupling in the symmetric NH_4^+ ion with diminished ^{14}N quadrupolar moment.[55] Precursor Isothio Bromide ligand does not show any NMR peaks in this region. NMR spectra of in situ generated 1D perovskite shows weak triplet peaks in the 6.92−7.43 ppm range which qualitatively matches to the peaks for ammonium chloride. Interestingly, similar triplet peaks are observed in the NMR spectra of the solution of isothiobromide in HBr when treated hydrothermally. Moreover, the NMR spectra have the same triplet peaks for 1D perovskite synthesized through 2 step process (6.96−7.47 ppm). Qualitative comparison of these NMR data (SI Figure S11) suggests that ammonium ions are present in the 1D perovskite structure. This identification of ammonium ions is in agreement with previous literature on incorporation of ammonium ions in 3D lead iodide perovskite.[56] A detailed NMR analysis following the complex mechanism of the ligand cleavage is not attempted here. The cleavage mechanism could yield a variety of ligands/moieties as can be attributed to the presence of the hydrogen on the "−C═N−H" group (with anticipated NMR peak at 9.14 ppm), and the hydrogen on the protonated amino group (with an anticipated NMR peak at 8.03 ppm). This may indicate that the product (ligand/moiety) obtained by the two-step method may contain mixed species rather than a single species of ligand. Hence, further mechanistic/analytical work on deciphering the cleavage mechanism is needed. Nonetheless, the single crystal structure data help clear identification of the ligand structure incorporated into the perovskite products.

CONCLUSIONS

Here, we demonstrate reduction/change of dimensionality/structure (2D/sheet →1D/chain) of lead bromide perovskite with 2-(2-aminoethyl)isothiourea dihydrobromide as precursor ligand by controlling the hydrothermal reaction conditions. Mechanistic studies and single crystal structure analysis reveal the 2D to 1D change in dimensionality upon increasing the hydrothermal reaction time and temperature. Interestingly, the resultant 1D chain perovskite is chiral and incorporates 2-(2-aminoethyldisulfanyl)ethanamine and ammonium ions as the ligands generated in situ due to hydrothermal cleavage of the precursor ligand. The 1D and 2D perovskite shows contrasting optical emission properties due to the reduction of dimensionality: 1D perovskite shows long-lived, self-trapped broad band emission, whereas 2D perovskite shows short-lived, band edge emission with long tail. The in situ conversion of the ligand structure and composition, which largely dictates the reduction of dimensionality, involves thermal cleavage of Isothio Bromide precursor ligand generating the modified ligand. This report highlights the importance of nature/structure, composition of the incorporated ligands in determining the dimensionality/structure and associated photophysical properties of these low dimensional perovskites.

ASSOCIATED CONTENT

Supporting Information

, . The Supporting Information is available free of charge at https://pubs.acs.org/doi/10.1021/acs.jpcc.9b11033.

TGA, Table of lifetimes, PXRD, grinding and annealing experiments, laser power dependent PL spectra, steady state PL at low temperatures, and ^{1}H NMR spectra (PDF)

Crystal structure data for 1D perovskite (CIF)

Crystal structure data for 2D perovskite (CIF)

checkCIF/PLATON report Structure factors have been supplied for datablock(s) iso_PbBr4_0ma_a (PDF)

checkCIF/PLATON report Structure factors have been supplied for datablock(s) mo_JK_13_0m_test (PDF)

Accession Codes

CCDC1942428 and CCDC1942429 contain the supplementary crystallographic data for this paper. These data can be obtained free of charge via www.ccdc.cam.ac.uk/data_request/

https://dx.doi.org/10.1021/acs.jpcc.9b11033
J. Phys. Chem. C 2020, 124, 1888−1897

cif, or by emailing data_request@ccdc.cam.ac.uk, or by contacting The Cambridge Crystallographic Data Centre, 12 Union Road, Cambridge CB2 1EZ, U.K.; fax: + 44 1223 336033.

AUTHOR INFORMATION

Corresponding Author

Janardan Kundu − *Indian Institute of Science Education and Research (IISER) Tirupati, Tirupati, India;* orcid.org/0000-0003-4879-0235; Email: janardan@iisertirupati.ac.in

Other Authors

Rangarajan Bakthavatsalam − *CSIR-National Chemical Laboratory, Pune, India, and Academy of Scientific and Innovative Research (AcSIR), Ghaziabad, India;* orcid.org/0000-0001-8473-8763

Muhammed P. U. Haris − *CSIR-National Chemical Laboratory, Pune, India, and Academy of Scientific and Innovative Research (AcSIR), Ghaziabad, India*

Samir R. Shaikh − *CSIR-National Chemical Laboratory, Pune, India, and Academy of Scientific and Innovative Research (AcSIR), Ghaziabad, India*

Amruta Lohar − *Savitribai Phule Pune University, Pune, India*

Ashutosh Mohanty − *Indian Institute of Science, Bengaluru, India*

Dhanashree Moghe − *Indian Institute of Technology Bombay, Mumbai, India*

Shivani Sharma − *Indian Institute of Science Education and Research (IISER) Pune, Pune, India*

Chinmoy Biswas − *Indian Institute of Technology Hyderabad, Kandi, India*

Sai Santhosh Kumar Raavi − *Indian Institute of Technology Hyderabad, Kandi, India*

Rajesh G. Gonnade − *CSIR-National Chemical Laboratory, Pune, India, and Academy of Scientific and Innovative Research (AcSIR), Ghaziabad, India;* orcid.org/0000-0002-2841-0197

Complete contact information is available at: https://pubs.acs.org/10.1021/acs.jpcc.9b11033

Author Contributions

The authors declare no competing financial interest.

Notes

The authors declare no competing financial interest.

ACKNOWLEDGMENTS

The authors thank Dr. S. Ghosh and Dr. S. R. Mahamuni for insightful discussion. R.B. acknowledges CSIR for senior research fellowship. R.S.S.K. acknowledges the financial support for the following project numbers BRICS/Pilot-Call2/IEEE-OSC/2018 (G) and SPARC/2018-2019/P301/SL. This work was supported by DST Grant No. SB/S2/RJN-61/2013.

REFERENCES

(1) Akkerman, Q. A.; Rainò, G.; Kovalenko, M. V.; Manna, L. Genesis, Challenges and Opportunities for Colloidal Lead Halide Perovskite Nanocrystals. *Nat. Mater.* **2018**, *17*, 394−405.

(2) Kovalenko, M. V.; Protesescu, L.; Bodnarchuk, M. I. Properties and Potential Optoelectronic Applications of Lead Halide Perovskite Nanocrystals. *Science* **2017**, *358*, 745−750.

(3) Li, W.; Wang, Z.; Deschler, F.; Gao, S.; Friend, R. H.; Cheetham, A. K. Chemically Diverse and Multifunctional Hybrid Organic−Inorganic Perovskites. *Nat. Rev. Mater.* **2017**, *2*, 16099.

(4) Tan, H.; et al. Efficient and Stable Solution-Processed Planar Perovskite Solar Cells Via Contact Passivation. *Science* **2017**, *355*, 722−726.

(5) Lin, H.; Zhou, C.; Tian, Y.; Siegrist, T.; Ma, B. Low-Dimensional Organometal Halide Perovskites. *ACS Energy Lett.* **2018**, *3*, 54−62.

(6) Saidaminov, M. I.; Mohammed, O. F.; Bakr, O. M. Low-Dimensional-Networked Metal Halide Perovskites: The Next Big Thing. *ACS Energy Lett.* **2017**, *2*, 889−896.

(7) Zhang, Y.; Liu, J.; Wang, Z.; Xue, Y.; Ou, Q.; Polavarapu, L.; Zheng, J.; Qi, X.; Bao, Q. Synthesis, Properties, and Optical Applications of Low-Dimensional Perovskites. *Chem. Commun.* **2016**, *52*, 13637−13655.

(8) Straus, D. B.; Kagan, C. R. Electrons, Excitons, and Phonons in Two-Dimensional Hybrid Perovskites: Connecting Structural, Optical, and Electronic Properties. *J. Phys. Chem. Lett.* **2018**, *9*, 1434−1447.

(9) Mitzi, D. B. Synthesis, Structure, and Properties of Organic-Inorganic Perovskites and Related Materials. *Prog. Inorg. Chem.* **2007**, *48*, 1−121.

(10) Mitzi, D. B. Templating and Structural Engineering in Organic−Inorganic Perovskites. *J. Chem. Soc., Dalton Trans.* **2001**, 1−12.

(11) Kieslich, G.; Sun, S.; Cheetham, A. K. Solid-State Principles Applied to Organic-Inorganic Perovskites: New Tricks for an Old Dog. *Chem. Sci.* **2014**, *5*, 4712−4715.

(12) Lemmerer, A.; Billing, D. G. Lead Halide Inorganic−Organic Hybrids Incorporating Diammonium Cations. *CrystEngComm* **2012**, *14*, 1954−1966.

(13) Mao, L.; Wu, Y.; Stoumpos, C. C.; Wasielewski, M. R.; Kanatzidis, M. G. White-Light Emission and Structural Distortion in New Corrugated Two-Dimensional Lead Bromide Perovskites. *J. Am. Chem. Soc.* **2017**, *139*, 5210−5215.

(14) Nazarenko, O.; Kotyrba, M. R.; Wörle, M.; Cuervo-Reyes, E.; Yakunin, S.; Kovalenko, M. V. Luminescent and Photoconductive Layered Lead Halide Perovskite Compounds Comprising Mixtures of Cesium and Guanidinium Cations. *Inorg. Chem.* **2017**, *56*, 11552−11564.

(15) Nazarenko, O.; Kotyrba, M. R.; Yakunin, S.; Aebli, M.; Rainò, G.; Benin, B. M.; Wörle, M.; Kovalenko, M. V. Guanidinium-Formamidinium Lead Iodide: A Layered Perovskite-Related Compound with Red Luminescence at Room Temperature. *J. Am. Chem. Soc.* **2018**, *140*, 3850−3853.

(16) Smith, M. D.; Karunadasa, H. I. White-Light Emission from Layered Halide Perovskites. *Acc. Chem. Res.* **2018**, *51*, 619−627.

(17) Yuan, Z.; Zhou, C.; Tian, Y.; Shu, Y.; Messier, J.; Wang, J. C.; van de Burgt, L. J.; Kountouriotis, K.; Xin, Y.; Holt, E.; et al. One-Dimensional Organic Lead Halide Perovskites with Efficient Bluish White-Light Emission. *Nat. Commun.* **2017**, *8*, 14051.

(18) Biswas, A.; Bakthavatsalam, R.; Shaikh, S. R.; Shinde, A.; Lohar, A.; Jena, S.; Gonnade, R. G.; Kundu, J. Efficient Broad-Band Emission from Contorted Purely Corner-Shared One Dimensional (1D) Organic Lead Halide Perovskite. *Chem. Mater.* **2019**, *31* (7), 2253−2257.

(19) Wang, X.; Meng, W.; Liao, W.; Wang, J.; Xiong, R.-G.; Yan, Y. Atomistic Mechanism of Broadband Emission in Metal Halideperovskites. *J. Phys. Chem. Lett.* **2019**, *10*, 501−506.

(20) Williams, R. T.; Song, K. S. The Self-Trapped Exciton. *J. Phys. Chem. Solids* **1990**, *51*, 679−716.

(21) Georgiev, M.; Mihailov, L.; Singh, J. Exciton Self-Trapping Processes. *Pure Appl. Chem.* **1995**, *67*, 447−456.

(22) Yangui, A.; et al. Optical Investigation of Broadband White-Light Emission in Self-Assembled Organic−Inorganic Perovskite $(C_6H_{11}NH_3)_2PbBr_4$. *J. Phys. Chem. C* **2015**, *119*, 23638−23647.

(23) Liu, Z.; Bekenstein, Y.; Ye, X.; Nguyen, S. C.; Swabeck, J.; Zhang, D.; Lee, S.-T.; Yang, P.; Ma, W.; Alivisatos, A. P. Ligand Mediated Transformation of Cesium Lead Bromide Perovskite Nanocrystals to Lead Depleted Cs_4PbBr_6 Nanocrystals. *J. Am. Chem. Soc.* **2017**, *139*, 5309−5312.
(24) Palazon, F.; Almeida, G.; Akkerman, Q. A.; De Trizio, L.; Dang, Z.; Prato, M.; Manna, L. Changing the Dimensionality of Cesium Lead Bromide Nanocrystals by Reversible Postsynthesis Transformations with Amines. *Chem. Mater.* **2017**, *29*, 4167−4171.
(25) Palazon, F.; Urso, C.; De Trizio, L.; Akkerman, Q.; Marras, S.; Locardi, F.; Nelli, I.; Ferretti, M.; Prato, M.; Manna, L. Postsynthesis Transformation of Insulating Cs_4PbBr_6 Nanocrystals into Bright Perovskite $CsPbBr_3$ through Physical and Chemical Extraction of CsBr. *ACS Energy Lett.* **2017**, *2*, 2445−2448.
(26) Akkerman, Q. A.; Park, S.; Radicchi, E.; Nunzi, F.; Mosconi, E.; De Angelis, F.; Brescia, R.; Rastogi, P.; Prato, M.; Manna, L. Nearly Monodisperse Insulator Cs_4PbX_6 (X = Cl, Br, I) Nanocrystals, Their Mixed Halide Compositions, and Their Transformation into $CsPbX_3$ Nanocrystals. *Nano Lett.* **2017**, *17*, 1924−1930.
(27) Udayabhaskararao, T.; et al. A Mechanistic Study of Phase Transformation in Perovskite Nanocrystals Driven by Ligand Passivation. *Chem. Mater.* **2018**, *30*, 84−93.
(28) Sharma, S. K.; Phadnis, C.; Das, T. K.; Kumar, A.; Kavaipatti, B.; Chowdhury, A.; Yella, A. Reversible Dimensionality Tuning of Hybrid Perovskites with Humidity: Visualization and Application to Stable Solar Cells. *Chem. Mater.* **2019**, *31*, 3111−3117.
(29) Ahmed, G. H.; et al. Pyridine-Induced Dimensionality Change in Hybrid Perovskite Nanocrystals. *Chem. Mater.* **2017**, *29*, 4393−4400.
(30) Zhou, C.; et al. Low Dimensional Organic Tin Bromide Perovskites and Their Photoinduced Structural Transformation. *Angew. Chem., Int. Ed.* **2017**, *56*, 9018−9022.
(31) Hautzinger, M. P.; Dai, J.; Ji, Y.; Fu, Y.; Chen, J.; Guzei, I. A.; Wright, J. C.; Li, Y.; Jin, S. Two-Dimensional Lead Halide Perovskites Templated by a Conjugated Asymmetric Diammonium. *Inorg. Chem.* **2017**, *56*, 14991−14998.
(32) Haris, M. P. U.; Bakthavatsalam, R.; Shaikh, S.; Kore, B. P.; Moghe, D.; Gonnade, R. G.; Sarma, D. D.; Kabra, D.; Kundu, J. Synthetic Control on Structure/Dimensionality and Photophysical Properties of Low Dimensional Organic Lead Bromide Perovskite. *Inorg. Chem.* **2018**, *57*, 13443−13452.
(33) Li, Y.; Zheng, G.; Lin, J. Synthesis, Structure, and Optical Properties of a Contorted < 110>-Oriented Layered Hybrid Perovskite: $C_3H_{11}SN_3PbBr_4$. *Eur. J. Inorg. Chem.* **2008**, *2008*, 1689−1692.
(34) Louvain, N.; Bi, W.; Mercier, N.; Buzaré, J. Y.; Legein, C.; Corbel, G. $Pb_nI_{4n+2}^{(2n+2)-}$ Ribbons (n = 3, 5) as Dimensional Reductions of 2d Perovskite Layers in Cystamine Cation Based Hybrids, Also Incorporating Iodine Molecules or Reversible Guest Water Molecules. *Dalton Trans.* **2007**, *2*, 965−970.
(35) Krishnamurthy, S.; Kour, P.; Katre, A.; Gosavi, S.; Chakraborty, S.; Ogale, S. Cystamine-Configured Lead Halide Based 2d Hybrid Molecular Crystals: Synthesis and Photoluminescence Systematics. *APL Mater.* **2018**, *6*, 114204.
(36) Bi, W.; Louvain, N.; Mercier, N.; Luc, J.; Rau, I.; Kajzar, F.; Sahraoui, B. A Switchable NLO Organic-Inorganic Compound Based on Conformationally Chiral Disulfide Molecules and $Bi(III)I_5$ Iodobismuthate Networks. *Adv. Mater.* **2008**, *20*, 1013−1017.
(37) Mercier, N.; Barres, A.-S.; Giffard, M.; Rau, I.; Kajzar, F.; Sahraoui, B. Conglomerate-to-True-Racemate Reversible Solid-State Transition in Crystals of an Organic Disulfide-Based Iodoplumbate. *Angew. Chem., Int. Ed.* **2006**, *45*, 2100−2103.
(38) Long, G.; et al. Spin Control in Reduced-Dimensional Chiral Perovskites. *Nat. Photonics* **2018**, *12*, 528−533.
(39) Chen, C.; Gao, L.; Gao, W.; Ge, C.; Du, X.; Li, Z.; Yang, Y.; Niu, G.; Tang, J. Circularly Polarized Light Detection Using Chiral Hybrid Perovskite. *Nat. Commun.* **2019**, *10*, 1−7.
(40) Ma, J.; Fang, C.; Chen, C.; Jin, L.; Wang, J.; Wang, S.; Tang, J.; Li, D. Chiral 2d Perovskites with a High Degree of Circularly Polarized Photoluminescence. *ACS Nano* **2019**, *13*, 3659−3665.
(41) Chen, W.; Zhang, S.; Zhou, M.; Zhao, T.; Qin, X.; Liu, X.; Liu, M.; Duan, P. Two-Photon Absorption-Based Upconverted Circularly Polarized Luminescence Generated in Chiral Perovskite Nanocrystals. *J. Phys. Chem. Lett.* **2019**, *10*, 3290−3295.
(42) Peng, Y.; Yao, Y.; Li, L.; Wu, Z.; Wang, S.; Luo, J. White-Light Emission in a Chiral One-Dimensional Organic-Inorganic Hybrid Perovskite. *J. Mater. Chem. C* **2018**, *6*, 6033−6037.
(43) Smith, M. D.; Jaffe, A.; Dohner, E. R.; Lindenberg, A. M.; Karunadasa, H. I. Structural Origins of Broadband Emission from Layered Pb−Br Hybrid Perovskites. *Chem. Sci.* **2017**, *8*, 4497−4504.
(44) Noh, M.; Kim, T.; Lee, H.; Kim, C.-K.; Joo, S.-W.; Lee, K. Fluorescence Quenching Caused by Aggregation of Water-Soluble Cdse Quantum Dots. *Colloids Surf., A* **2010**, *359*, 39−44.
(45) Bowers, M. J.; McBride, J. R.; Rosenthal, S. J. White-Light Emission from Magic-Sized Cadmium Selenide Nanocrystals. *J. Am. Chem. Soc.* **2005**, *127*, 15378−15379.
(46) Tongay, S.; Suh, J.; Ataca, C.; Fan, W.; Luce, A.; Kang, J. S.; Liu, J.; Ko, C.; Raghunathanan, R.; Zhou, J.; et al. Defects Activated Photoluminescence in Two-Dimensional Semiconductors: Interplay between Bound, Charged, and Free Excitons. *Sci. Rep.* **2013**, *3*, 2657.
(47) Schmidt, T.; Lischka, K.; Zulehner, W. Excitation-Power Dependence of the near-Band-Edge Photoluminescence of Semiconductors. *Phys. Rev. B: Condens. Matter Mater. Phys.* **1992**, *45*, 8989−8994.
(48) Mao, L.; Guo, P.; Kepenekian, M.; Hadar, I.; Katan, C.; Even, J.; Schaller, R. D.; Stoumpos, C. C.; Kanatzidis, M. G. Structural Diversity in White Light Emitting Hybrid Lead Bromide Perovskites. *J. Am. Chem. Soc.* **2018**, *140*, 13078−13088.
(49) Gautier, R.; Massuyeau, F.; Galnon, G.; Paris, M. Lead Halide Post-Perovskite-Type Chains for High-Efficiency White-Light Emission. *Adv. Mater.* **2019**, *31*, 1807383.
(50) Cui, B.-B.; Han, Y.; Huang, B.; Zhao, Y.; Wu, X.; Liu, L.; Cao, G.; Du, Q.; Liu, N.; Zou, W.; et al. Locally Collective Hydrogen Bonding Isolates Lead Octahedra for White Emission Improvement. *Nat. Commun.* **2019**, *10*, 5190.
(51) Thirumal, K.; et al. Morphology-Independent Stable White-Light Emission from Self-Assembled Two-Dimensional Perovskites Driven by Strong Exciton−Phonon Coupling to the Organic Framework. *Chem. Mater.* **2017**, *29*, 3947−3953.
(52) Viswanath, A. K.; Lee, J. I.; Kim, D.; Lee, C. R.; Leem, J. Y. Exciton-Phonon Interactions, Exciton Binding Energy, and Their Importance in the Realization of Room Temperature Semiconductor Lasers Based on Gan. *Phys. Rev. B: Condens. Matter Mater. Phys.* **1998**, *58*, 16333.
(53) Netzel, C.; Hoffmann, V.; Wernicke, T.; Knauer, A.; Weyers, M.; Kneissl, M.; Szabo, N. Temperature and Excitation Power Dependent Photoluminescence Intensity of Gainn Quantum Wells with Varying Charge Carrier Wave Function Overlap. *J. Appl. Phys.* **2010**, *107*, No. 033510.
(54) Dohner, E. R.; Jaffe, A.; Bradshaw, L. R.; Karunadasa, H. I. Intrinsic Whitelight Emission from Layered Hybrid Perovskites. *J. Am. Chem. Soc.* **2014**, *136*, 13154−13157.
(55) Witanowski, M.; Webb, G. A. *Nitrogen NMR*; Plenum Press: London, 1973.
(56) Hamill, J. C., Jr.; Sorli, J. C.; Pelczer, I.; Schwartz, J.; Loo, Y.-L. Acid-Catalyzed Reactions Activate DMSO as a Reagent in Perovskite Precursor Inks. *Chem. Mater.* **2019**, *31*, 2114−2120.

https://dx.doi.org/10.1021/acs.jpcc.9b11033
J. Phys. Chem. C 2020, 124, 1888−1897